PHYSICAL REVIEW B **91**, 014437 (2015)

Jahn-Teller driven perpendicular magnetocrystalline anisotropy in metastable ruthenium

Dorj Odkhuu,[1,2] S. H. Rhim,[1,3,*] Noejung Park,[4] Kohji Nakamura,[5] and Soon Cheol Hong[1,†]

[1]*Department of Physics and Energy Harvest Storage Research Center, University of Ulsan, Ulsan, 680-789, Republic of Korea*
[2]*Department of Physics, Incheon National University, Incheon, 406-772, Republic of Korea*
[3]*Department of Physics and Astronomy, Northwestern University, Evanston, Illinois 60208, USA*
[4]*Department of Physics, Ulsan National Institute of Science and Technology, Ulsan, 689-798, Republic of Korea*
[5]*Department of Physics Engineering, Mie University, Tsu, Mie 514-8507, Japan*

(Received 2 May 2014; revised manuscript received 3 December 2014; published 30 January 2015)

A metastable phase of body-centered-tetragonal ruthenium (bct Ru) is identified to exhibit a large perpendicular magnetocrystalline anisotropy (PMCA), whose energy E_{MCA} is as large as 150 μeV/atom, which is two orders of magnitude greater than those of 3d magnetic metals. Further investigation over the range of tetragonal distortion suggests that the appearance of magnetism in the bct Ru is governed by the Jahn-Teller spit e_g orbitals. Moreover, from band analysis, MCA is mainly determined by an interplay between two e_g states, $d_{x^2-y^2}$ and d_{z^2} states, as a result of level reversal associated with tetragonal distortion.

DOI: 10.1103/PhysRevB.91.014437 PACS number(s): 75.30.Gw, 75.50.Cc, 75.70.Tj

I. INTRODUCTION

Physics phenomena originating from spin-orbit interactions, such as magnetocrystalline anisotropy (MCA), Rashba-type interactions, or topological insulators, have attracted huge attention for their intriguing physics as well as their great potential for spintronics applications [1–5]. In particular, MCA, where one particular direction of the magnetization is energetically preferred, offers opportunities in spintronics such as magnetic random access memory (MRAM), spin-transfer torque (STT), magneto-optics, to list a few. With recent advances in fabrication techniques, the search for materials with large MCA, more preferably, perpendicular MCA (PMCA), has been very intensive.

In particular, ferromagnetic films that can provide PMCA are indispensable constituents in STT memory that utilizes spin-polarized tunneling current to switch magnetization [6]. Two criteria have to be satisfied for the practical usage of high-density magnetic storage: low switching current (I_{SW}) and thermal stability. A small volume is favored to lower I_{SW}, but it is detrimental to thermal stability. However, the shortcoming of a small volume can be compensated by large MCA while still retaining thermal stability. On the other hand, low magnetization will offer the advantage of a reduced stray field in real devices. Therefore, the exploration for materials with high anisotropy and small magnetization would be one favorable direction to minimize I_{SW} and at the same time to maximize the thermal stability.

In the framework of perturbation theory [7], E_{MCA} is determined by the spin-orbit interaction between occupied and unoccupied states as

$$E_{\mathrm{MCA}}^{\sigma\sigma'} \approx \xi^2 \sum_{o,u} \frac{|\langle o^{\sigma}|\ell_Z|u^{\sigma'}\rangle|^2 - |\langle o^{\sigma}|\ell_X|u^{\sigma'}\rangle|^2}{\epsilon_{u,\sigma'} - \epsilon_{o,\sigma}}, \quad (1)$$

where o^{σ} ($u^{\sigma'}$) and $\epsilon_{o,\sigma}$ ($\epsilon_{u,\sigma'}$) represent occupied (unoccupied) eigenstates and eigenvalues for each spin state, $\sigma,\sigma' = \uparrow, \downarrow$, respectively; ξ is the strength of spin-orbit coupling (SOC).

As the electronic structure of magnetic materials with non-negigible MCA is mainly dominated by d electrons, it would be worthwhile to see how the energy levels of d orbitals evolve in different crystal symmetries, as illustrated in Fig. 1. For bcc Ru with $c/a = 1$, the cubic symmetry splits five d orbitals into doublets (e_g) and triplets (t_{2g}). When the lattice changes from high-symmetric body-centered to tetragonal with lower symmetry, additional Jahn-Teller splitting may offer more freedom to provide more energy differences in Eq. (1). More specifically, the tetragonal distortion further splits these e_g and t_{2g} levels into two irreducible representations: e_g into two singlets a_1 (d_{z^2}) and b_1 ($d_{x^2-y^2}$), and t_{2g} into a singlet b_2 (d_{xy}) and a doublet e ($d_{yz,xz}$), where their relative order is determined by c/a, which is either larger or smaller than unity.

Metals with 4d and 5d valence electrons possess inherently larger SOC than conventional 3d metals. The search for magnetism in these transition metals has a long history. The fact that Pd and Pt barely miss the Stoner criteria to become ferromagnetic (FM) has incurred enormous efforts to realize magnetism in several multilayers and interfaces of 4d metals by adjusting the volumes or lattice constants, thereby, increasing the density of states (DOS) at the Fermi level (E_F), $N(E_F)$, due to a narrowed bandwidth, would meet the Stoner criteria. Hence, 4d and 5d metals with large SOC as well as magnetism would be favorable candidates to realize large MCA.

A previous theoretical study has suggested that ferromagnetism in Ru is feasible in a body-centered-cubic (bcc) structure when the lattice is expanded by 5% [8]. Other studies predicted that magnetism can occur in Rh and Pd with volume changes [9,10]. However, theoretically proposed magnetism associated with volume changes in 4d metals has not been fully confirmed experimentally. Nevertheless, with remarkable advances in current fabrication techniques, various types of lattices are now accessible with a diverse choice of substrates. In particular, the bct Ru film has been successfully fabricated on the Mo (110) substrate, whose lattice constants are $a = 3.24$ Å and $c/a = 0.83$, as identified by x-ray electron diffraction [11]. Later, a theoretical calculation argued that magnetism can exist in bct Ru for $c/a = 0.84$ with a moment of 0.4μ_B/atom [12].

*sonny@ulsan.ac.kr
†schong@ulsan.ac.kr

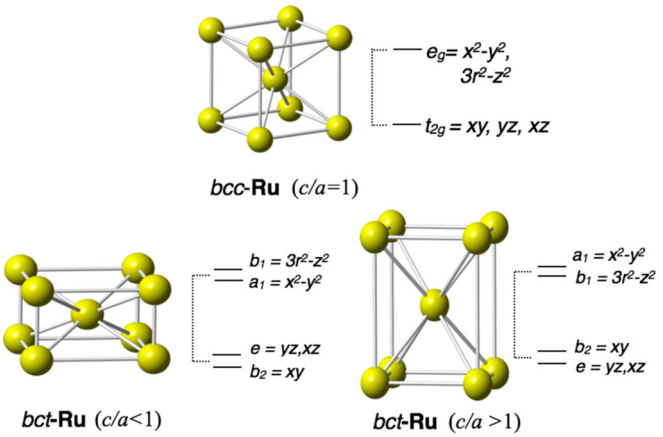

FIG. 1. (Color online) Schematic presentation of the Jahn-Teller splitting of d electrons. In the cubic symmetry, such as bcc ($c/a = 1$), the d orbital splits into doublets (e_g) and triplets (t_{2g}). Tetragonal distortion further splits e_g into a_1 and b_1; t_{2g} splits into a singlet b_2 and a doublet e, where their relative order is shown depending on whether c/a is greater or smaller than unity.

In this paper, we present that in an identified metastable phase of bct Ru, $E_{\rm MCA}$ can be as large as 150 μeV/atom, which is two orders of magnitude greater than those in 3d magnetic metals. The magnetic instability driven by this tetragonal distortion is discussed in connection with the Stoner criteria. Furthermore, we show that magnetism as well as MCA are governed mainly by the Jahn-Teller split e_g orbitals.

II. COMPUTATIONAL DETAILS

Density functional calculations were performed using the highly precise full-potential linearized augmented plane wave (FLAPW) method [13]. For the exchange-correlation potential, the generalized gradient approximation (GGA) was employed as parametrized by Perdew, Burke, and Ernzerhof (PBE) [14]. Energy cutoffs of 16 and 256 Ry were used for wave function expansions and potential representations. Charge densities and potential inside muffin-tin (MT) spheres were expanded with lattice harmonics $\ell \leqslant 8$ with a MT radius of 2.4 a.u. To obtain reliable values of MCA energy ($E_{\rm MCA}$), calculations with high precision are indispensable. A $40 \times 40 \times 40$ mesh in the irreducible Brillouin zone wedge is used for k point summation. A self-consistent criteria of 1.0×10^{-5} $e/(\text{a.u.})^3$ was imposed for calculations, where convergence with respect to the numbers of basis functions and k points was also seriously checked [15,16]. For the calculation of $E_{\rm MCA}$, the torque method [7,17] was employed to reduce computational costs, whose validity and accuracy have been proved in conventional FM materials [18–23].

III. RESULTS AND DISCUSSION

Equilibrium lattice constants of hexagonal-closed-packed (hcp), face-centered-cubic (fcc), and bcc Ru are summarized in Table I, which are in good agreement with experiments [11,24] and previous work [12]. The hcp structure is the most stable phase, as Ru crystallizes in hcp. However, the energy difference between hcp and fcc, 0.07 eV/atom, is very small, which reflects the feature of the closed packed structures of the two but with different stacking sequences. In Fig. 2(a), the total energy of nonmagnetic (NM) bct Ru as a function of tetragonal distortion (c/a) is plotted for a fixed volume of the equilibrium bcc structure. Our result reproduces that given by Watanabe *et al.*[12]: There is a global minimum at $c/a = 1.41$ corresponding to the fcc structure. There are two other extrema, a local maximum and minimum at $c/a = 1$ and $c/a = 0.84$, respectively. In particular, the local minimum at $c/a = 0.84$ suggests the existence of a metastable phase, as discussed in Ref. [12]. Further calculations of total energy of the bct structure as a function of both a and c/a confirms that the local minimum is at $a = 3.25$ Å and $c/a = 0.84$, consistent with the fixed volume calculation of the bcc structure.

In Fig. 2(b), $N(E_F)$ of non-spin-polarized and magnetic moments of the spin-polarized calculation are plotted as a function of the lattice constant. The onset of magnetism in the bcc phase occurs at $a = 3.10$ Å, which corresponds to a 1.1% expansion of the lattice constant, *or* a 3.3% expansion of the volume, as consistent with Ref. [8]. In order for the magnetic instability in the bcc phase to satisfy the Stoner criteria, $IN(E_F) \geqslant 1$, and from the fact that the Stoner factor I of a particular atom does not differ substantially in different crystal structures, we estimate $I = 0.46$ eV for Ru from $N(E_F) = 2.18$ eV^{-1}.

On the other hand, as shown in Fig. 2(c), the energy difference between the NM and FM states ($\Delta E = E_{\rm NM} - E_{\rm FM}$) and the magnetic moment reveal almost the same trends as c/a changes. ΔE of the bcc and fcc phases are negligibly small, thus both phases are nonmagnetic. When $c/a < 1.1$ but $c/a \neq 1$, the bct Ru is magnetic ($\Delta E > 0$), whereas when $c/a > 1.1$, it is nonmagnetic. In particular, $c/a = 0.84$ gives $\Delta E = 35$ meV/atom with a magnetic moment as high as $0.6\mu_B$, which is larger than $0.40\mu_B$ in Ref. [12]. Interestingly,

TABLE I. Calculated equilibrium lattice parameters, a (in Å) and c/a, and total energy difference ΔE (in eV/atom) of hcp, fcc, bcc, and bct Ru with respect to the total energy of the hcp structure. Experimental and previous theoretical results are also given for comparison.

	hcp		fcc		bcc		bct		
	Present	Experiment[a]	Present	Previous[b]	Present	Previous	Present	Previous[b]	Experiment[a]
a	2.70	2.70	3.84	3.84	3.07	3.06	3.25	3.25	3.24
c/a	1.58	1.58	1.09	1.00	1.00	1.00	0.84	0.83	0.83
ΔE	0.0		0.07	0.13	0.56	0.65	0.48	0.55	

[a]Shiiki *et al.* [11].
[b]Watanabe *et al.* [12].

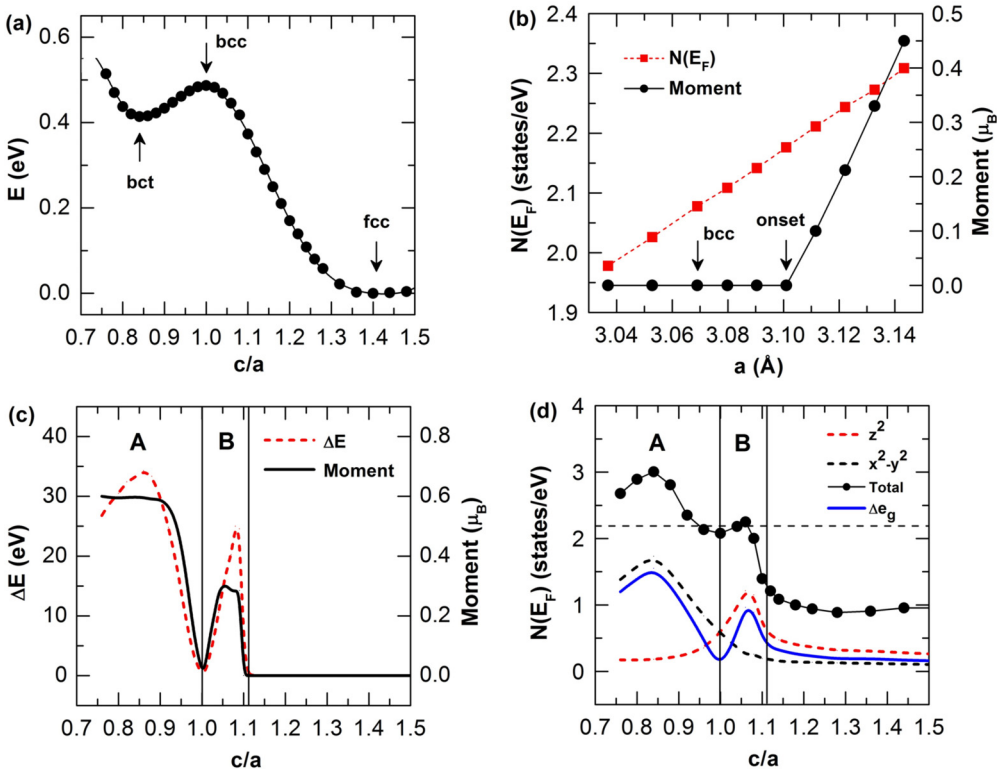

FIG. 2. (Color online) (a) Total energy with respect to the fcc structure ($c/a = 1.41$) of nonmagnetic bct Ru upon the tetragonal distortion (c/a) in fixed volume of the bcc structure. The equilibria c/a for bct, bcc, and fcc are denoted. (b) $N(E_F)$ of non-spin-polarized calculations (red squares), and the magnetic moment of bcc Ru as a function of the uniform lattice constant a (black circles). The arrow denotes the equilibrium lattice constant of bcc Ru. (c) The energy difference $\Delta E = E_{\mathrm{NM}} - E_{\mathrm{FM}}$ (red dotted line) and magnetic moments (black solid line) as a function of c/a. The tetragonal distortion is classified into two regions, A and B, by $c/a < 1$ or > 1. (d) $N(E_F)$ of NM bct Ru as a function of c/a. Total $N(E_F)$, those from d_{z^2}, $d_{x^2-y^2}$, and the absolute value of the difference of the two e_g orbitals, denoted as Δe_g, are shown as black solid circles, a black dotted line, a red dashed line, and a blue solid line, respectively.

the magnetic moment of the bct Ru exhibits a reentrance behavior for $c/a > 1$, as predicted by Schönecker *et al.* [25]. In region A ($c/a < 1$), the magnetic moment decreases as c/a increases, whereas magnetism reappears when c/a just passes unity, which eventually vanishes for $c/a > 1.1$.

The total DOS and those from e_g orbitals at E_F as a function of c/a are plotted in Fig. 2(d) for the NM bct Ru. Most contributions come from the Jahn-Teller split e_g orbitals, whose difference in DOS is also plotted: It resembles the magnetic moment shown in Fig. 2(c). Moreover, among the Jahn-Teller split e_g orbitals, $d_{x^2-y^2}(d_{z^2})$ dominates the other for $c/a < 1$ ($c/a > 1$).

The partial DOS (PDOS) of d orbitals are shown in Fig. 3 for the spin-polarized cases, where the trivial $c/a = 1$ is omitted. The prominent peaks at $c/a = 0.84$ are mainly from the $d_{x^2-y^2}$ states with occupied (unoccupied) peaks in the majority (minority) spin bands, while the peaks in the d_{z^2} states evolve as c/a increases. Contributions from the t_{2g} states are rather featureless.

For simplicity, we assign the energy difference of the peaks in the e_g states, $d_{x^2-y^2}$ for $c/a < 1$ and d_{z^2} for $c/a > 1$, respectively, as the exchange splitting. Then, as c/a increases, the exchange splittings are 1.02, 1.05, 0.80, and 0.66 eV for $c/a = 0.84$, 0.90, 0.96, and 1.06, respectively, which qualitatively reflects magnetism of the bct Ru. From this, the exchange splitting is mainly determined by one of the Jahn-Teller split e_g orbitals.

In addition to magnetism, the bct Ru exhibits large MCA. The angle-dependent total energy in a tetragonal symmetry is expressed in the most general form, $E_{\mathrm{tot}}(\theta,\varphi) = E_0 + k_1 \sin^2\theta + k_2 \sin^4\theta + k_3 \sin^4\theta \cos 4\varphi$, where θ and φ are polar and azimuthal angles, respectively, and $k_1 = 100$, $k_2 = -1$, and $k_3 \ll 1$ μeV. The small value of k_3 indicates a negligible φ dependence. $E_{\mathrm{MCA}} = E_{\mathrm{tot}}(\theta = 90^\circ) - E_{\mathrm{tot}}(\theta = 0^\circ)$ as a function of the tetragonal distortion c/a is shown in Fig. 4(a). Here, $E_{\mathrm{MCA}} = 150$ μeV/atom at $c/a = 0.80$, and $E_{\mathrm{MCA}} = 100$ μeV/atom for the local minimum ($c/a = 0.84$), which is two orders of magnitude greater than conventional $3d$ magnetic metals. As the strength of the tetragonal distortion changes, E_{MCA} changes not only in magnitude but also in sign. In region A, E_{MCA} becomes negative near $c/a \approx 0.9$ and reaches -100 μeV/atom around $c/a = 0.96$, whereas in region B, $E_{\mathrm{MCA}} > 0$: PMCA is restored. Hence, the strength of the tetragonal distortion c/a influences the magnetic moments as well as E_{MCA}.

E_{MCA} is decomposed into different spin channels following Eq. (1), as shown in Fig. 4(b) for bct Ru with $c/a = 0.84$, 0.90, 0.96, and 1.06, respectively. For $\sigma\sigma' = \uparrow\uparrow$ or $\downarrow\downarrow$, the

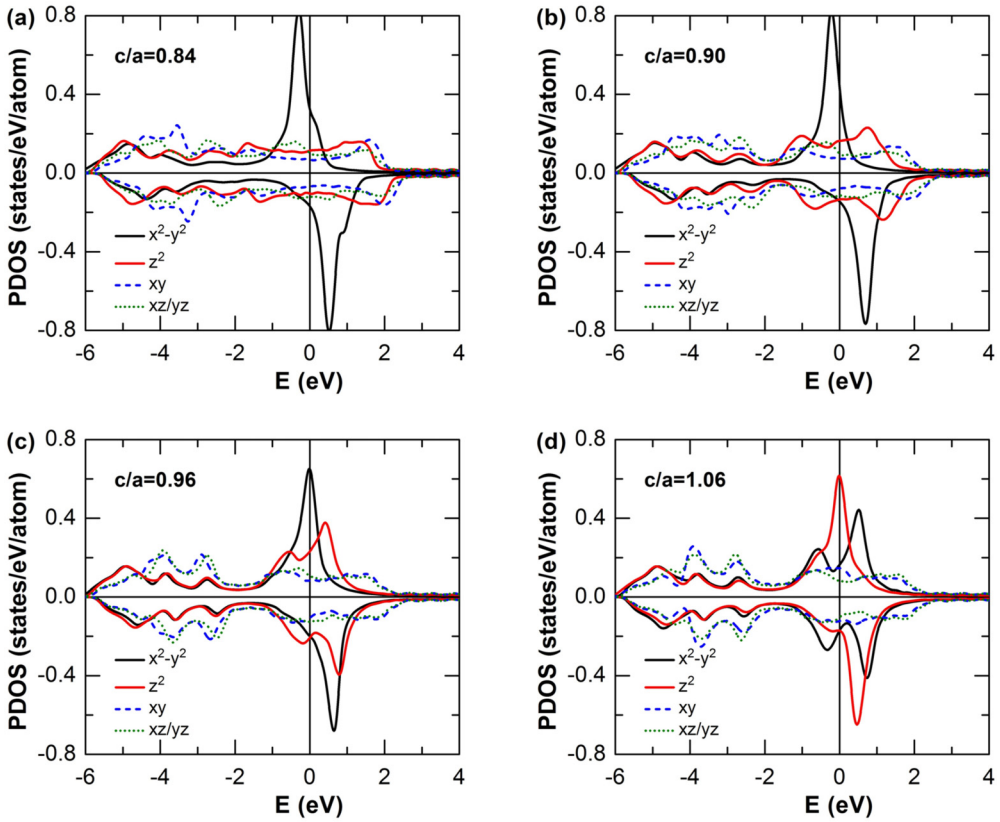

FIG. 3. (Color online) Orbital-decomposed DOS of the d orbital for spin-polarized calculations of bct Ru at $c/a =$ (a) 0.84, (b) 0.90, (c) 0.96, and (d) 1.06, respectively. The d-orbital states are shown in different colors: red (d_{z^2}), black ($d_{x^2-y^2}$), blue (d_{xy}), and green ($d_{xz,yz}$), respectively.

positive (negative) contribution to E_{MCA} is determined by the SOC interaction between the occupied and unoccupied states with the same (different by one) magnetic quantum number (m) through the ℓ_Z (ℓ_X) operator. For $\sigma\sigma' = \uparrow\downarrow$, Eq. (1) has opposite sign, so the positive (negative) contribution comes from the ℓ_X (ℓ_Z) coupling.

From the spin-channel decomposition of E_{MCA}, one notes that there is no dominant spin channel. This feature differs from the $3d$ transition metals, where a particular spin channel, i.e., the $\downarrow\downarrow$ channel, dominantly contributes to the positive value through the SOC matrix $\langle x^2 - y^2|\ell_Z|xy\rangle$, with negligible ones from the ℓ_X matrices [7,26]. When $c/a = 0.84$, the $\downarrow\downarrow$ channel gives the largest contribution, while those from other channels are smaller than half of the $\downarrow\downarrow$ channel with opposite signs. As c/a increases, the $\downarrow\downarrow$-channel contribution is reduced, which turns negative for $c/a > 1$. MCA almost vanishes for $c/a =$

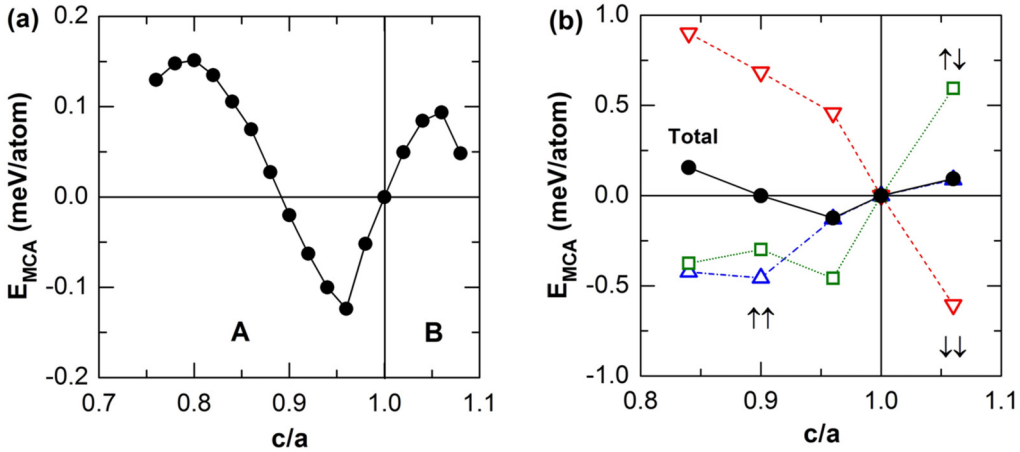

FIG. 4. (Color online) (a) MCA energy dependence on c/a for bct Ru, where A and B are defined as in Fig. 2(b). (b) Spin channel decomposed and total E_{MCA} of bct Ru for various c/a. The black circles denote total MCA. The upper (lower) triangles denote the $\uparrow\uparrow$ ($\downarrow\downarrow$) channel, and squares denote the $\uparrow\downarrow$ channel.

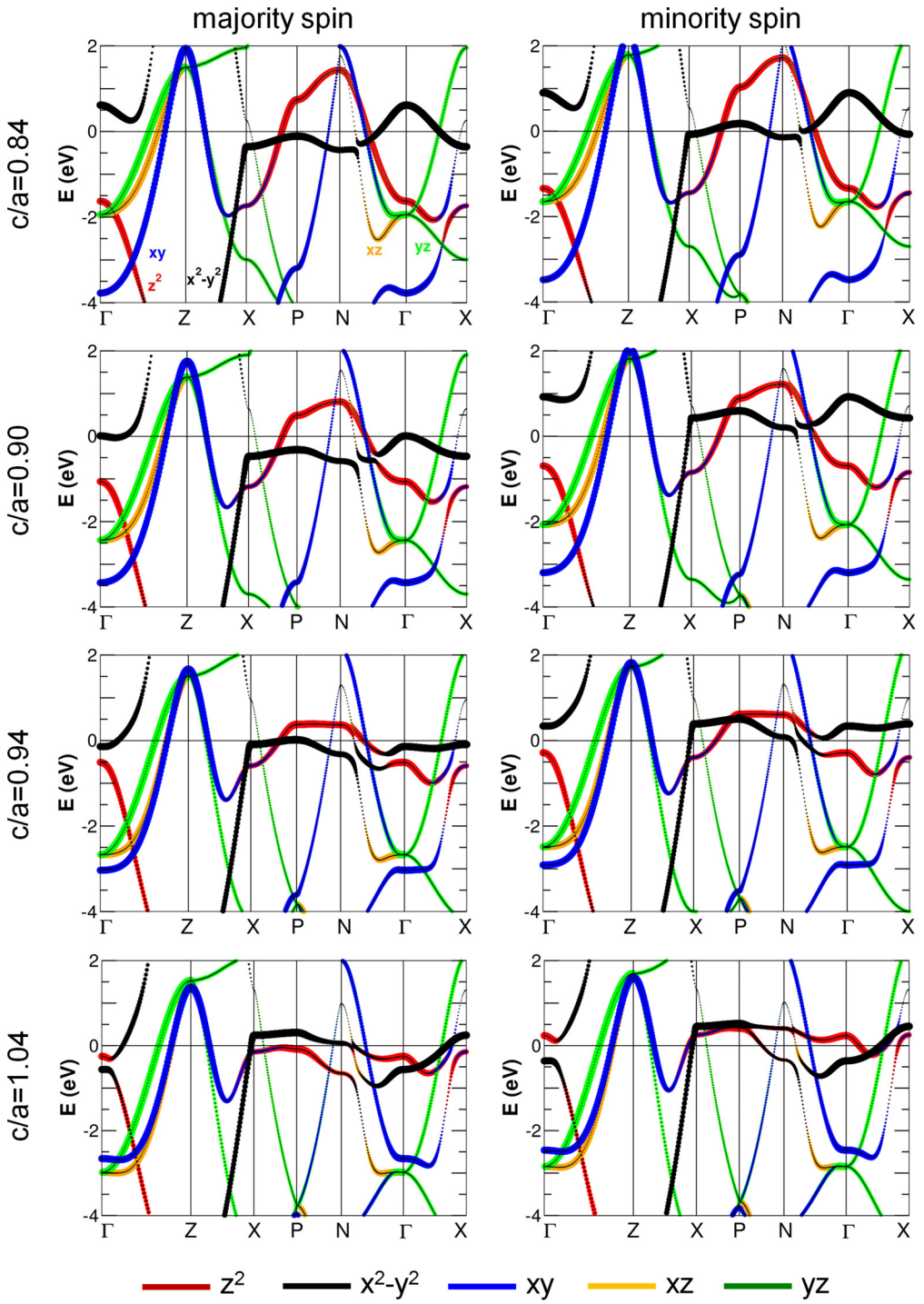

FIG. 5. (Color online) Band structures of bct Ru for $c/a = 0.84, 0.90, 0.96$, and 1.06 for the majority and minority spin states. The d-orbital states are shown in different colors: red (d_{z^2}), black ($d_{x^2-y^2}$), blue (d_{xy}), orange (d_{xz}), and green (d_{yz}), respectively.

0.90 and becomes negative for $c/a = 0.96$. On the other hand, for $c/a = 1.06$, the $\uparrow\downarrow$ and $\downarrow\downarrow$ channels contribute almost the same magnitudes with opposite signs, so just the $\uparrow\uparrow$-channel contribution remains.

To obtain more insights, the band structure is plotted in Fig. 5 with d-orbital projection, where the size of the symbols is proportional to their weights. All the bands along Γ-Z-X are highly dispersive, whereas those along X-P-N-Γ-X are less dispersive with a rather flat feature from the $d_{x^2-y^2}$ and d_{z^2} states. The level reversals between e_g states, $d_{x^2-y^2}$ and d_{z^2}, are well manifested, while t_{2g} states are relatively rigid with respect to tetragonal distortion. It is a formidable task to identify the role of each individual SOC matrix for each c/a. However, from the spin-channel decomposed MCA [Fig. 4(b)], each spin channel changes its sign when c/a becomes greater than unity, where the level reversal occurs between $d_{x^2-y^2}$ and d_{z^2}.

For a simple analysis, we express the $\downarrow\downarrow$ channel as

$$E(\downarrow\downarrow) = \frac{|\langle x^2-y^2|\ell_Z|xy\rangle|^2}{\epsilon_{x^2-y^2}-\epsilon_{xy}} - \frac{|\langle x^2-y^2|\ell_X|xz\rangle|^2}{\epsilon_{x^2-y^2}-\epsilon_{xz}} - \frac{|\langle z^2|\ell_X|xz\rangle|^2}{\epsilon_{z^2}-\epsilon_{xz}}. \quad (2)$$

We focus along X-P-N-Γ-X, where e_g's are unoccupied. The $\langle yz|\ell_Z|xz\rangle$ contributions are neglected due to the rigidity of the t_{2g} states as well as their small contribution to E_{MCA} owing to the large energy denominator. From the fact that $E(\downarrow\downarrow) > 0$ when $c/a = 0.84$ with the largest value, we can infer that the first term in Eq. (2) should be larger than the other two, where the largest occurs along P-N. [See the Supplementary Material (SM) for the k-resolved MCA analysis [27].]

As c/a increases but $c/a < 1$, the empty d_{z^2} band moves downward while the empty $d_{x^2-y^2}$ band goes upward with respect to E_F. As a result, the third term is enhanced due to a smaller energy denominator. Hence, $E(\downarrow\downarrow)$ decreases but remains positive. When $c/a > 1$, however, the level reversal between e_g states pushes d_{z^2} above E_F and $d_{x^2-y^2}$ below E_F along N-Γ-X. The former provides an additional negative contribution while the latter reduces the positive contribution. As a consequence, $E(\downarrow\downarrow) < 0$ for $c/a > 1$. The sign behavior of the $\uparrow\downarrow$ component, $E(\uparrow\downarrow)$, is completely opposite to $E(\downarrow\downarrow)$, as all terms in Eq. (2) take opposite signs [7]. For the $\uparrow\uparrow$ component when $c/a < 1$, we focus near P-N. The largest positive contribution in the $\downarrow\downarrow$ component is significantly reduced in the $\uparrow\uparrow$ channel because the empty $d_{x^2-y^2}$ band in the minority spin is occupied in the majority spin, and the empty d_{z^2} band contributes negatively. Thus, $E(\uparrow\uparrow) < 0$. When $c/a > 1$, the occupancies of the e_g states are reversed again due to the level reversal, therefore $E(\uparrow\uparrow) > 0$. We want to point out that the level reversal between the $d_{x^2-y^2}$ and the d_{z^2} states not only affects the sign behavior of MCA but also the exchange splitting in DOS. The above argument of the sign behavior is more clearly supported by the k-resolved MCA analysis. (See SM Figs. S1–S5 [27].)

IV. CONCLUSION

In summary, a metastable phase of bct Ru has been identified to exhibit a large PMCA, which is two orders of magnitude greater than conventional magnetic metals. In the context of spintronics applications, this large anisotropy, along with low magnetization and small volume, would be key factors to realize materials with a low switching current and high thermal stability. Magnetism of bct Ru is mainly governed by the Jahn-Teller split e_g states. As the strength of the tetragonal distortion changes, the magnetism of bct Ru shows an interesting reentrance behavior for $1 < c/a < 1.1$. The tetragonal distortion accompanies MCA changes in both magnitudes and signs, as a result of the level reversal between $d_{x^2-y^2}$ and d_{z^2}.

ACKNOWLEDGMENTS

This work is supported by the Basic Science Research Program (2010-0008842) and Priority Research Centers Program (2009-0093818) through the National Research Foundation (NRF) funded by the Korean Ministry of Education (KME). N.P. is supported by the Basic Science Research Program (2013R1A1A2007910) through the NRF funded by the KME. K.N. acknowledges support from a Grant-in-Aid for Scientific Research (No. 24540344) from the Japanese Society for the Promotion of Science. D.O. and S.H.R. contributed equally to this work.

[1] M. Z. Hasan and C. L. Kane, Rev. Mod. Phys. **82**, 3045 (2010).
[2] X.-L. Qi and S.-C. Zhang, Rev. Mod. Phys. **83**, 1057 (2011).
[3] S. Wolf, D. Aschwalom, R. Buhrman, J. Daughton, S. von Molnár, M. Roukes, A. Y. Chtchelkanova, and D. Tregor, Science **294**, 1488 (2001).
[4] I. Žutić, J. Fabian, and S. das Sarma, Rev. Mod. Phys. **76**, 323 (2004).
[5] A. Brataas, A. D. Kent, and H. Ohno, Nat. Mater. **11**, 372 (2012).
[6] J. Z. Sun, Phys. Rev. B **62**, 570 (2000).
[7] D. S. Wang, R. Q. Wu, and A. J. Freeman, Phys. Rev. B **47**, 14932 (1993).
[8] M. Kobayashi, T. Kai, N. Takano, and K. Shiiki, J. Phys. Condes. Matter **7**, 1835 (1995).
[9] V. L. Moruzzi and P. M. Marcus, Phys. Rev. B **39**, 471 (1989).
[10] H. Chen, N. E. Brener, and J. Callaway, Phys. Rev. B **40**, 1443 (1989).
[11] K. Shiiki and O. Hio, Jpn. J. Appl. Phys. **36**, 7360 (1997).
[12] S. Watanabe, T. Komine, T. Kai, and K. Shiiki, J. Magn. Magn. Mater. **220**, 277 (2000).
[13] E. Wimmer, H. Krakauer, M. Weinert, and A. J. Freeman, Phys. Rev. B **24**, 864 (1981).
[14] J. P. Perdew, K. Burke, and M. Ernzerhof, Phys. Rev. Lett. **77**, 3865 (1996).
[15] Y. Mokrousov, G. Bihlmayer, S. Heinze, and S. Blügel, Phys. Rev. Lett. **96**, 147201 (2006).
[16] S. C. Hong and J. I. Lee, J. Korean Phys. Soc. **52**, 1099 (2008).
[17] X. Wang, R. Wu, D.-S. Wang, and A. J. Freeman, Phys. Rev. B **54**, 61 (1996).
[18] R. Q. Wu and A. J. Freeman, J. Magn. Magn. Mater. **200**, 498 (1999).
[19] D. Odkhuu and S. C. Hong, J. Appl. Phys. **107**, 09A945 (2010).
[20] Y. N. Zhang and R. Q. Wu, Phys. Rev. B **82**, 224415 (2010).
[21] D. Odkhuu, W. S. Yun, S. H. Rhim, and S. C. Hong, Appl. Phys. Lett. **98**, 152502 (2011).
[22] D. Odkhuu, W. S. Yun, and S. C. Hong, J. Appl. Phys. **111**, 063911 (2012).
[23] D. Odkhuu, S. H. Rhim, N. Park, and S. Hong, Phys. Rev. B **88**, 184405 (2013).
[24] D. R. Lide, *Handbook of Chemistry and Physics: A Ready Reference Book of Chemical and Physical Data*, 83rd ed. (CRC, New York, 2002).
[25] S. Schönecker, M. Richter, K. Koepernik, and H. Eschrig, Phys. Rev. B **85**, 024407 (2012).
[26] K. Hotta, K. Nakamura, T. Akiyama, T. Ito, T. Oguchi, and A. J. Freeman, Phys. Rev. Lett. **110**, 267206 (2013).
[27] See Supplemental Material at http://link.aps.org/supplemental/10.1103/PhysRevB.91.014437 for k-resolved MCA.